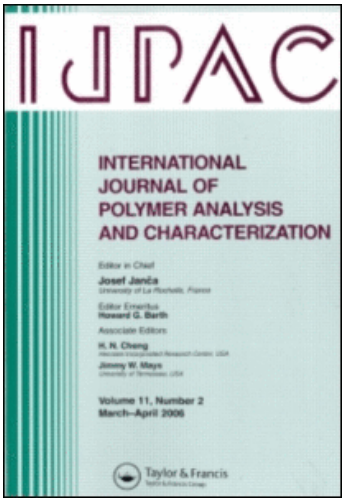

International Journal of Polymer Analysis and Characterization
Publication details, including instructions for authors and subscription information:
http://www.informaworld.com/smpp/title~content=t713646643

Isothermal Crystallization Behavior of Poly(ε-Caprolactone) Diol/Functionalized-Multiwalled Carbon Nanotube Composites

R. N. Jana[a]; C. Im[a]
[a] Department of Chemistry, Konkuk University, Seoul, Korea

To cite this Article Jana, R. N. and Im, C.(2009) 'Isothermal Crystallization Behavior of Poly(ε-Caprolactone) Diol/Functionalized-Multiwalled Carbon Nanotube Composites', International Journal of Polymer Analysis and Characterization, 14: 5, 418 — 436
To link to this Article: DOI: 10.1080/10236660903031074
URL: http://dx.doi.org/10.1080/10236660903031074

International Journal of Polymer Anal. Charact., 14: 418–436, 2009

ISSN: 1023-666X print
DOI: 10.1080/10236660903031074

Taylor & Francis
Taylor & Francis Group

Isothermal Crystallization Behavior of Poly(ε-Caprolactone) Diol/Functionalized-Multiwalled Carbon Nanotube Composites

R. N. Jana and C. Im
Department of Chemistry, Konkuk University, Seoul, Korea

Abstract: Isothermal crystallization behavior of poly (ε-caprolactone) diol (PCL)/functionalized-multiwalled carbon nanotube (f-MWNTs) composites at three different temperatures (30°, 35°, 40°C), with varying molecular weights (MW) of PCL (2000, 4000, 8000 g/mol) and loadings of f-MWNTs (0, 0.1, 1.0, 5.0 wt.%), was studied by differential scanning calorimetry (DSC), polarized optical microscopy (POM), and X-ray diffraction methods. DSC isotherm showed that introduction of f-MWNTs into PCL induced a heterogeneous nucleation in the crystallization growth process, thereby lowering the activation energy for the crystallization process appreciably. POM showed the spherulite structure of neat PCL, whereas the composites showed the spherulite structure containing f-MWNTs at the center, indicating nucleating action of f-MWNTs in the crystallization process. The spherulite size decreased but its number increased with increasing weight proportion of f-MWNTs and MW of PCL.

Keywords: Activation energy; Differential scanning calorimetry; Isothermal crystallization; Multiwalled carbon nanotubes; Poly(ε-caprolactone) diol; Scanning electron microscopy

Submitted 25 March 2009; accepted 24 April 2009.
This research was supported by the 2008 KU Brain Pool Program of Konkuk University, Korea.
Correspondence: R. N. Jana, Department of Chemistry, Konkuk University, 1 Hwayang-dong, Gwangjin-gu, Seoul 143-701, Korea. E-mail: rabindra@konkuk.ac.kr

INTRODUCTION

Since their discovery,[1] multiwalled carbon nanotubes (MWNTs) have received much interest and are being used in different fields of applications, e.g., nanocomposites,[2,3] electronic devices,[4,5] actuators,[6,7] and field emitters.[8,9] Though MWNT-based polymer nanocomposites have improved mechanical and electrical properties compared to the neat polymers, there may be a phase separation between the polymer matrix and MWNTs.[10] This problem can be coped with by the formation of a chemical bond between the MWNTs and the polymer so that there may be better bonding and hence better stress transfer properties.[11–13] In order to understand the factors affecting the service properties of the composites, the study of their crystallization behavior is important. It is reported that the MWNTs present in the composites may help in the crystallization process of the polymer by acting as a nucleating agent to reduce the crystallization time as well as the overall crystallization rate.[14] From the literature, it is found also that most of the research work has been devoted to study the crystallization behavior under non-isothermal conditions, whereas the crystallization at isothermal conditions is important, because at these conditions we can gain insight into the actual crystallization process without any temperature thrust.

Poly(ε-caprolactone) diol (PCL), a biodegradable polymer, is chosen for our present study because of its potential application in medical fields, though it has a major drawback due to its high crystallinity and low thermal stability.[15] There are several reports on its biodegradation and crystallization behavior[16,17]; however, the reinforcement mechanism of MWNTs to PCL is still not clear. The effect of molecular weight (MW) on the crystallization behavior for different polymers, such as poly (ethylene terephtalate) (PET),[18–22] polyethylene,[23–26] poly(p-phenylene sulfide),[27] and polypropylene,[28] has been reported. In general, both the overall growth rate of crystallization and the resulting crystallinity decrease with increasing MW, except in the low MW range[19,29] or at low cooling rate conditions. For example, if the MW of PET is lower than 8000, its overall crystallization rate increases with MW[19]; otherwise, its overall crystallization rate decreases with increasing MW. Again, there are several reports on isothermal crystallization behavior of PCL/MWNT composites,[30–32] but there is no report that deals with the effect of MW of PCL on its crystallization behavior for the composite system.

We have used different weight proportions of f-MWNTs with different MW of PCL to prepare PCL/f-MWNT composites and to find the effect of MW and weight proportion of f-MWNTs on isothermal crystallization behavior of the composites at three different temperatures (30°, 35°, 40°C). To improve the dispersion of MWNTs in PCL matrix, we at first treated MWNTs with H_2SO_4:HNO_3 (3:1 v/v) solution, which

produced carboxylic acid groups at the surface of the MWNTs,[33–35] then treated them with thionyl chloride to give acylchloride functionalized MWNTs (f-MWNTs), and finally different weight proportions of f-MWNTs were melt-mixed with PCL. The isothermal crystallization kinetics of the composites was studied by differential scanning calorimetry (DSC), polarized optical microscopy (POM), and X-ray diffraction.

EXPERIMENTAL SECTION

Materials

MWNTs of grade CM-95 were supplied by Iljin Nanotech Co. (Seoul, Korea), with an average diameter of 10–15 nm, length of 10–20 μm, and a purity of 95%. PCL with different MW (2000, 4000, and 8000 g/mol) was received from Solvay Co. (Cheshire, UK). Thionyl chloride, nitric acid, and sulfuric acid were of laboratory grade reagents.

Preparation of PCL/f-MWNT Composites

Taking about 2.0 g of MWNTs in a 500 mL flask equipped with a condenser, 20 mL of 60% HNO_3 and 60 mL of 98% H_2SO_4 were added with vigorous stirring (Scheme 1). It was sonicated using a high-power ultrasonic processor for 10 min, stirred for 1 h under reflux (110°C), then a dense brown gas was collected and treated with a NaOH aqueous solution connected to the condenser. After cooling to room temperature, the reaction mixture was diluted with 100 mL of distilled water and vacuum filtered through a filter paper (Minipore 1.0 μm). The solid was dispersed in 100 mL of water and filtered again. The dispersion, filtering, and washing steps were continued until the filtrate became neutral. The filtered solid was then washed with 50 mL of acetone to remove most of the water from the sample. Then the solid was dried under vacuum at 60°C for 24 h to get the carboxylated MWNTs.

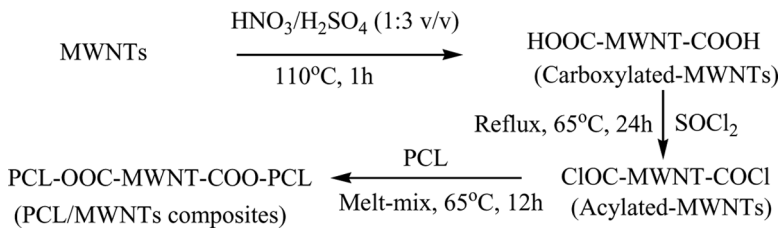

Scheme 1. Synthesis route for PCL/f-MWNT composites.

Taking 20 mL of thionyl chloride ($SOCl_2$) with 1.0 g of carboxylated MWNTs in a flask, reflux was continued at 65°C for 24 h. The residual $SOCl_2$ was removed by reducing the pressure during the distillation and then the produced acylchloride-functionalized MWNTs (f-MWNTs) were melt-mixed at 65°C for 12 h with a required quantity of PCL in a flask at constant mechanical stirring to get the desired composites (Table I).

Characterization

Fourier transform-infrared (FT-IR) measurements were performed using a Jasco FT-IR 300E by attenuated total reflectance method. Raman spectroscopy was used to investigate the structural changes of MWNTs before and after the acid treatment. A 632.8 nm (1.96 eV) He-Ne laser was used as the light source, and optical filters were used to adjust the power of the laser. The illuminated spot on the sample surface was focused to a diameter of approximately 2 mm. The resolution of the Raman spectra was 1 cm^{-1}. Raman signals were collected using a charge-coupled device (CCD) that was cooled by liquid nitrogen. DSC measurements were carried out using a TA Instruments 2010 thermal analyzer in nitrogen atmosphere at a flow rate of 50 mL/min. All the specimens were weighed in the range of 5–10 mg. The specimens were heated up to 100°C at a heating rate of 20°C/min and held there for 20 min to remove the residual crystallinity, then cooled quickly to the chosen crystallization temperatures in the range of 30°–40°C. The heat of fusion versus time for isothermal crystallization was recorded. Wide-angle X-ray diffraction measurements using CuK_α radiation and a nickel filter were carried out in an X-ray diffractometer (Bruker AXS). The diffraction was recorded in the angular range of $2\theta = 0°–40°$ at a scanning speed 5°/min. The area ratio of crystalline peaks to the total area of crystalline and amorphous peaks was used as the measure of crystallinity. A polarized optical

Table I. Composition for PCL/MWNT composites

	MW of PCL (g/mol)			
Sample code	2000 (wt.%)	4000 (wt.%)	8000 (wt.%)	f-MWNTs
M-1	100	0	0	0
M-2	0	100	0	0
M-3	0	0	100	0
M-4	0	100	0	0.1
M-5	0	100	0	1.0
M-6	0	100	0	5.0

microscope (POM) (Eclipse LV 100 POL) from Nikon Corporation (Tokyo, Japan) equipped with a hot stage (LTS 350) from Linkam Scientific Instruments Ltd. (Waterfield, Surrey, UK) was used.

RESULTS AND DISCUSSION

Interaction between PCL and f-MWNTs

Figure 1 shows the first-order Raman spectra of the pristine MWNTs and carboxylated MWNTs. The pristine MWNTs have two peaks at 1321 and 1578 cm^{-1}, assigned to the disorder mode (D-band) and tangential mode (G-band), respectively.[36] In the carboxylated MWNTs, the D-band appears at a somewhat higher value (1332 cm^{-1}) whereas the G-band remains almost the same (1579 cm^{-1}). The D-band intensity increases in carboxylated MWNTs compared to that in the pristine MWNTs, and its peak intensity ratio ($I_D/I_G \approx 1.58$) also exceeds that of pristine MWNTs ($I_D/I_G \approx 1.25$). This may be due to the destruction of double bond in the MWNTs by means of the strong oxidizing acids.

FT-IR spectrum of pristine MWNTs shows a weak peak at 1638 cm^{-1} corresponding to C = O stretching, indicative of few carboxylic acid groups present in the pristine MWNTs (Figure 2). After the oxidation with the acids mixture, C = O stretching is shifted to 1696 cm^{-1} and

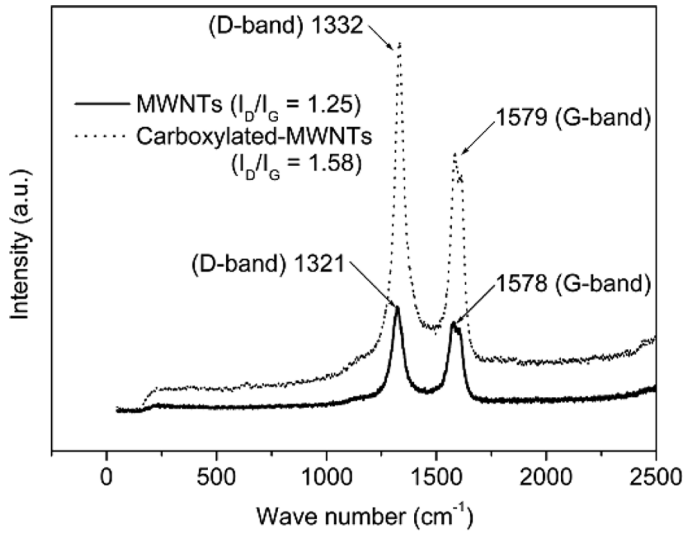

Figure 1. Raman spectra of pristine MWNTs and carboxylated MWNTs.

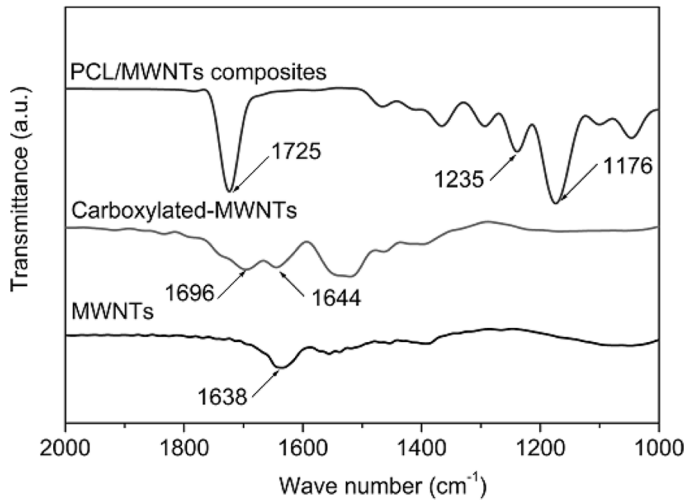

Figure 2. FT-IR spectra of pristine MWNTs, carboxylated MWNTs, and PCL/f-MWNT composite (M-4).

1644 cm^{-1}. These peaks may be due to free carbonyl groups and hydrogen-bonded carbonyl groups of the f-MWNTs, respectively.[37] After the reaction with PCL along with a strong carbonyl peak at 1725 cm^{-1} of PCL, two new peaks at 1235 cm^{-1} and 1176 cm^{-1} appeared. The peaks at 1235 cm^{-1} and 1176 cm^{-1} may be due to the formation of C-O bond by the reaction between acylchloride groups (–COCl) of f-MWNTs and hydroxyl groups (-OH) of PCL. Thus there is a covalent bond formation between PCL and f-MWNTs as outlined in Scheme 1.

Figure 3 shows the scanning electron microscopy (SEM) micrographs of pristine MWNTs, PCL/pristine MWNT, and PCL/f-MWNT composite. Here, both the pristine MWNTs and PCL/pristine MWNT composite exhibit noticeable aggregation of the nanotubes as shown in Figure 3(a) and (b), whereas if f-MWNTs are mixed with PCL, they

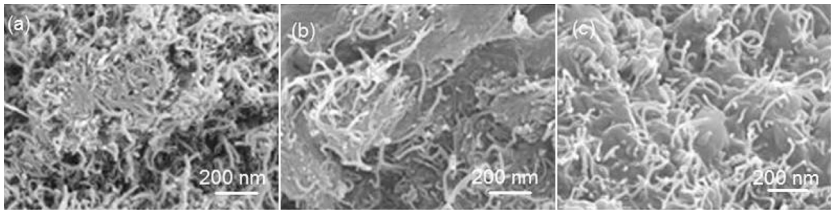

Figure 3. SEM photomicrographs of (a) pristine MWNTs, (b) PCL/pristine MWNT composite, and (c) PCL/f-MWNT composite (M-4).

almost uniformly mixed and dispersed throughout the PCL matrix (Figure 3(c)). Thus, the improved dispersion may be due to chemical bond formation between PCL and f-MWNTs.

Isothermal Crystallization Kinetics

The isothermal crystallization kinetics of PCL and PCL/f-MWNT composites can be analyzed using the Avrami equation[38]:

$$1 - X_t = \exp(-kt^n) \quad \text{or,} \quad \ln[-\ln(1 - X_t)] = n \ln t + \ln k \qquad (1)$$

where X_t is the relative crystallinity at time t, obtained from the area of the exothermic peak in the DSC isotherm at crystallization time t divided by the total area under the exothermic peak, n is the Avrami exponent, and k is the crystallization rate constant. Both n and k depend on the nucleation and growth mechanisms of spherulites. The n and k values could be directly obtained with Equation (1) from the slope and intercept of the best fitting line. Figure 4 shows the DSC scan of neat PCL and PCL/f-MWNT composites, and the variation of relative crystallinity (X_t) with time is shown in Figure 5(a). Figure 5(b) shows a plot of $\ln[-\ln(1-X_t)]$ versus $\ln t$ for different MW of neat PCL and the composites. The different n and k values are reported in Table II.

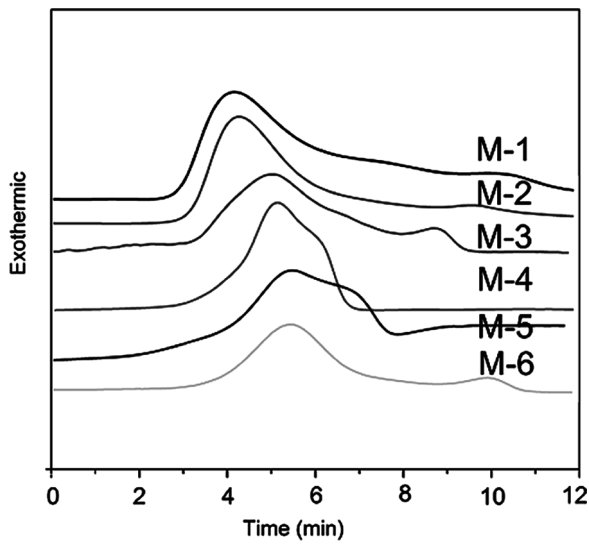

Figure 4. DSC scan of different PCL and PCL/f-MWNT composites.

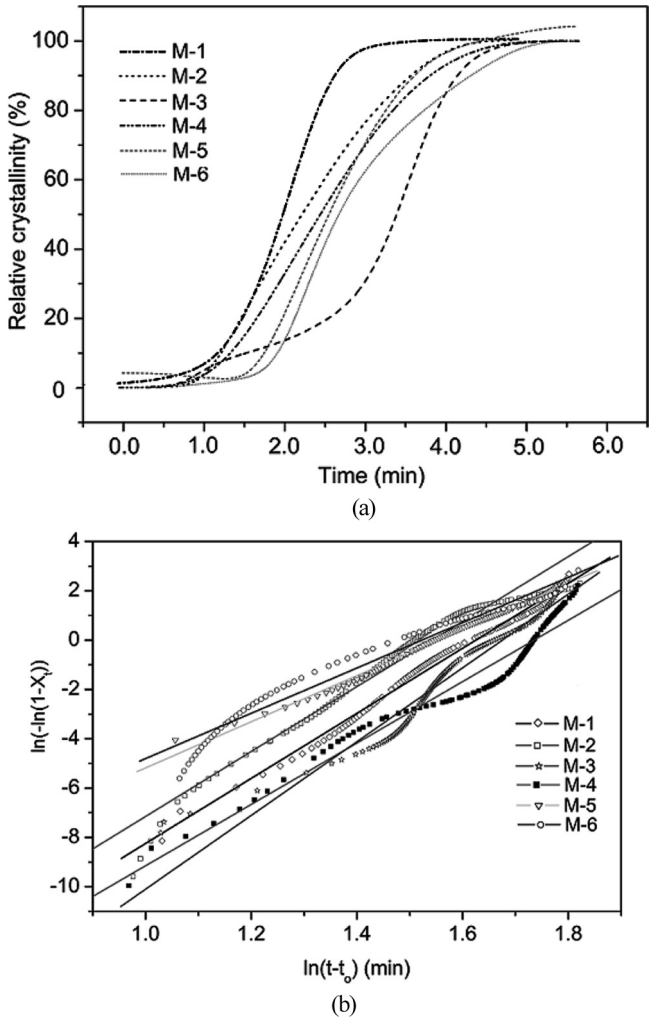

Figure 5. Plots of (a) relative crystallinity vs. crystallization time and (b) $\ln(-\ln(1-X_t))$ vs. $\ln t$ of different neat PCL and PCL/f-MWNT composites.

Effect of MW of PCL

From Table II, it is clear that the n values increase with increase in crystallization temperature and MW of PCL, and in all cases n values are higher than 3, indicating that the crystallization process proceeded in more than three modes. The nonintegral n values may be due to the presence of crystalline branching and/or two-stage crystal growth during the crystallization process and/or a mixed growth and nucleation process.[39]

Table II. Values of n and k at different crystallization temperatures

Sample code	n values			k values			$t_{1/2}$ at 35°C (min)
	30°C	35°C	40°C	30°C	35°C	40°C	
M-1	3.10	3.28	3.35	2.59×10^{-1}	2.18×10^{-1}	1.54×10^{-1}	1.9
M-2	3.71	3.83	3.95	2.25×10^{-1}	9.70×10^{-2}	2.56×10^{-2}	2.2
M-3	3.76	3.86	3.98	3.58×10^{-2}	1.49×10^{-2}	4.53×10^{-3}	3.5
M-4	2.86	3.12	3.32	3.34	1.85	7.25×10^{-1}	2.4
M-5	2.52	2.64	2.85	8.51×10^{-1}	6.67×10^{-1}	2.54×10^{-1}	2.6
M-6	2.15	2.32	2.38	4.58×10^{-1}	8.49×10^{-2}	3.61×10^{-2}	2.7

Here, the k values decrease with increasing crystallization temperature as well as with increasing MW of PCL. At a high temperature, a polymeric molecule has high kinetic energy, which results in it being crystallized. Again, as the MW of PCL increases the chain mobility to form a crystal is restricted. Thus, the isothermal half-crystallization time ($t_{1/2}$ at 35°C) as measured from Figure 5(a) also increases with increase in MW of PCL. For instance, $t_{1/2}$ for PCL with MW of 2000 (i.e., M-1 sample) and 8000 (i.e., M-3 sample) are 1.9 min and 3.5 min, respectively (Table II). Again, for a constant MW (e.g., 4000) of PCL, the crystallization process completes within 6–8 min as confirmed in Figure 6. The crystallization time observed from POM is somewhat higher than that obtained from the DSC studies because of experimental error.

Effect of Weight Proportion of f-MWNTs

The plots of $\ln[-\ln(1-X_t)]$ versus $\ln t$ for M-2, M-3, and M-4 composites are shown also in Figure 5(b) and their crystallization parameters are listed in Table II. The n values of the composites are in the range of 2.15–3.32, which are lower than that of PCL. Therefore, these results indicate that introducing f-MWNTs into PCL significantly influences heterogeneous nucleation induced by a change in the crystal growth process from three-dimensional crystal growth to mixed two-dimensional and three-dimensional spherulitic growth. Moreover, the crystallization rate constant also decreases with increasing crystallization temperature because of a gradual decrease in the degree of supercooling. The values of k decrease with increasing f-MWNT content in the composites, indicating a significant increase in the heterogeneous nucleation for PCL/f-MWNT composites. Thus the values of $t_{1/2}$ increase with increase in wt.% of MWNTs in the composites (Table II). For the composite with a constant weight proportion (e.g., M-6 composite) the crystallization time is about 8–14 min (Figure 7), which is somewhat higher than that of neat PCL. It is also found that with the increase of f-MWNTs in the composites, the

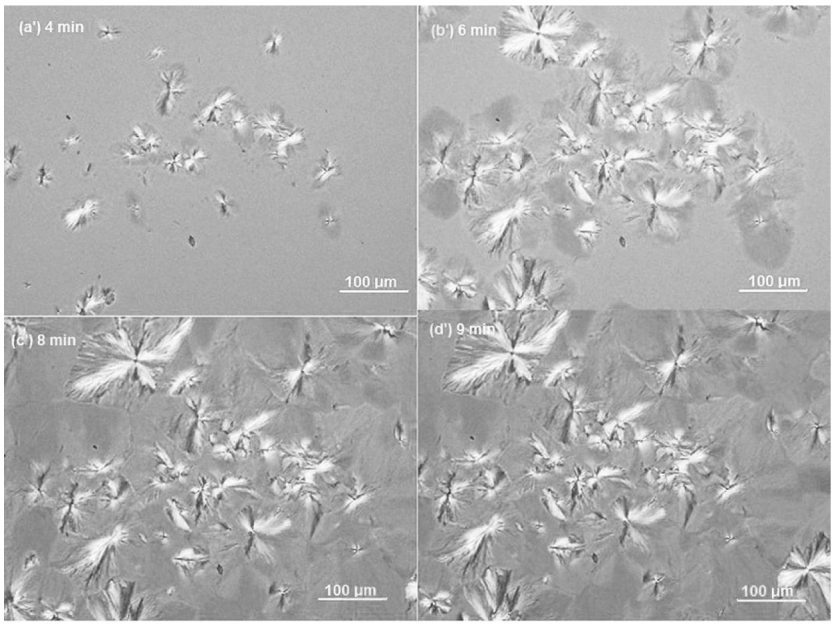

Figure 6. POM of M-2 sample at different times: (a) 4 min, (b) 6 min, (c) 8 min, and (d) 9 min during crystallization isothermally at 35°C.

crystallinity of the composites decreases as confirmed by the X-ray diffraction studies (Figure 8). The degree of crystallinity (X_c) for the composite is 35.5%, whereas for neat PCL (MW = 4000) it is about 36.3%.[33]

Activation Energy for Crystallization Process

Activation energy for the crystallization process can be measured from the kinetic rate constant (k) using the following Arrhenius type equation:

$$\ln k = \ln k_0 - \Delta E/RT \tag{2}$$

where k_0 is a temperature-independent pre-exponential factor; ΔE is the total activation energy, which consists of the nucleation activation energy (ΔF) and the transport activation energy (ΔE^*) (ΔF is the free energy of formation of the critical-size crystal nuclei at the proposed crystallization temperature (T_c) and ΔE^* refers to the activation energy required to transport molecular segments across the phase boundary to the crystallization surface); and R is the universal gas constant. Arrhenius plots of ln k against $1/T_c$ for neat PCL and PCL/f-MWNT composites are shown in Figure 9(a), and the activation energy is determined from the slope of the plots.

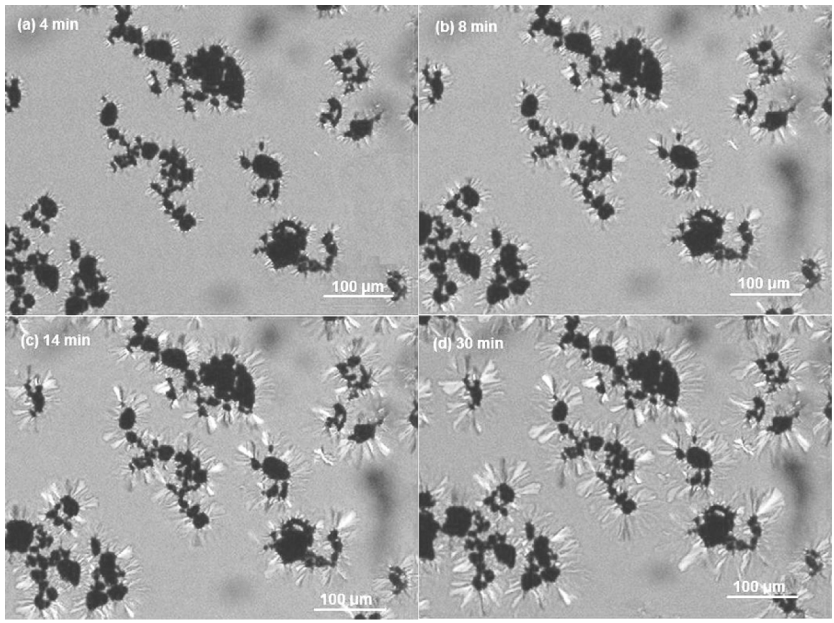

Figure 7. POM of M-6 composite at different times: (a) 4 min, (b) 8 min, (c) 14 min, and (d) 30 min during crystallization isothermally at 35°C.

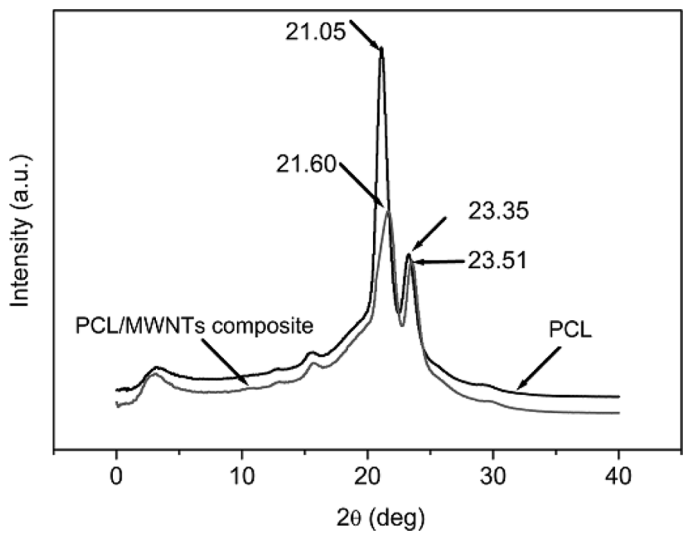

Figure 8. Wide-angle X-ray diffraction patterns of M-2 and M-6 composites.

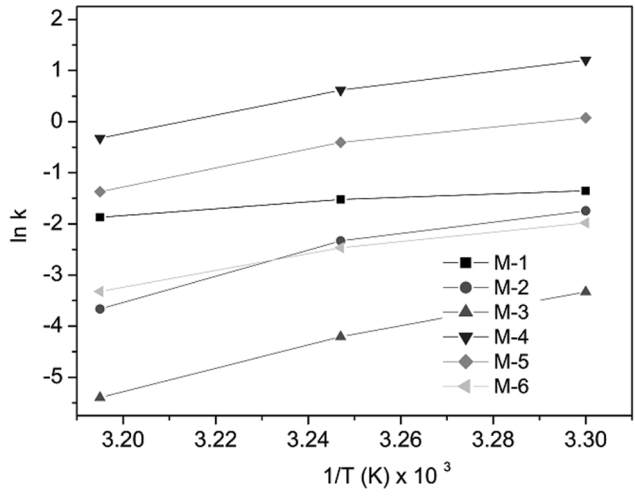

(a)

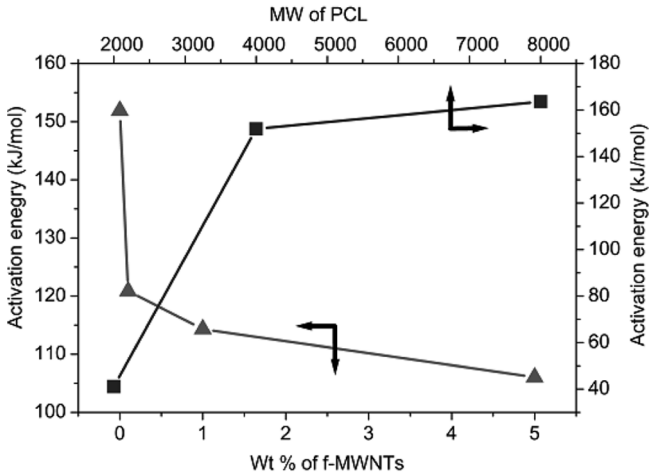

(b)

Figure 9. Plots of (a) lnk vs. 1/T and (b) activation energy with wt.% of f-MWNTs and MW of PCL.

Effect of MW of PCL

The activation energy as obtained from Figure 9(a) is plotted in Figure 9(b). With increasing MW of PCL, there is an increase in activation energy for the crystallization process. This is because as the MW

increases, the chain mobility decreases and the crystallization process becomes energetically forbidden.

Effect of Weight Proportion of f-MWNTs

Activation energy for the crystallization process is dependent also on the content of f-MWNTs in the composites. The activation energy drastically decreases with the presence of 0.1 wt.% f-MWNTs in the composites and then this decrease is marginal. For instance, ΔE for neat PCL with MW 4000 (i.e., M-2 sample) is 151.8 kJ/mol, whereas for the composite containing only 0.1 wt.% f-MWNTs (i.e., M-4 composite) it reduces to 120.8 kJ/mol (Figure 9(b)). The result indicates that the addition of 0.1 wt.% f-MWNTs to PCL probably induces heterogeneous nucleation, thus showing a lower ΔE value. The addition of more f-MWNTs to the PCL matrix is expected to cause more heterogeneous nucleation, i.e., lower ΔE values. However, we have found that the decrease is marginal with further addition of f-MWNTs (>0.1 wt.%) in the composites because of more steric hindrance, which reduces the transport ability of polymer chains during the crystallization process.

Crystal Growth Process

The crystal growth process was characterized with the help of POM. The temperature dependence of the linear growth rate (G) may also be determined from the following equation[29]:

$$G = G_0 \, exp\left[\frac{-U^*}{R(T_c - T_\infty)}\right] exp\left[\frac{-K_g}{T_c(\Delta T)f}\right] \tag{3}$$

where G_0 is a pre-exponential term, U^* is the diffusional activation energy for the transport of crystallizable segments at the liquid-solid interface, T_∞ is the hypothetical temperature below which viscous flow ceases, and $f = 2T_c/(T_m^0 + T_c)$ is a correction factor that accounts for the change in the enthalpy of fusion of the perfect crystal (ΔH_f^0) with temperature. The nucleation constant (K_g) contains contributions from the surface free energies, and it can be obtained from the following equation:

$$K_g = \frac{4b\sigma\sigma_e T_m^0}{\beta k \Delta H_f^0} \tag{4}$$

where b is the distance between two adjacent fold planes; σ and σ_e are the lateral and fold surface free energies, respectively; k is the

Boltzmann constant; and β is a parameter that depends on the regime of crystallization.

Effect of MW of PCL

Figure 10(a)–(c) shows POM photomicrographs of neat PCL of different MW after isothermal crystallization at 35°C for 30 min from their melts. The micrograph exhibits a typical Maltese-cross spherulite. The average crystal size is 198.45, 98.88, and 93.30 μm for PCL with MW of 2000, 4000, and 8000 g/mole, respectively (Figure 10(a)–(c)). The decrease in crystal size with increase in MW of PCL is due to the lower transport ability of the longer polymeric chains as explained earlier. For a constant MW of PCL (e.g., 4000), the crystal size increases with the time of crystallization as can be seen in Figure 11a. The crystallization process completes within 6–8 min.

Effect of Weight Proportion of f-MWNTs

Figure 10(d) shows the POM photomicrograph of M-5 composite crystallized at 35°C for 30 min from its melt. The average crystal size is

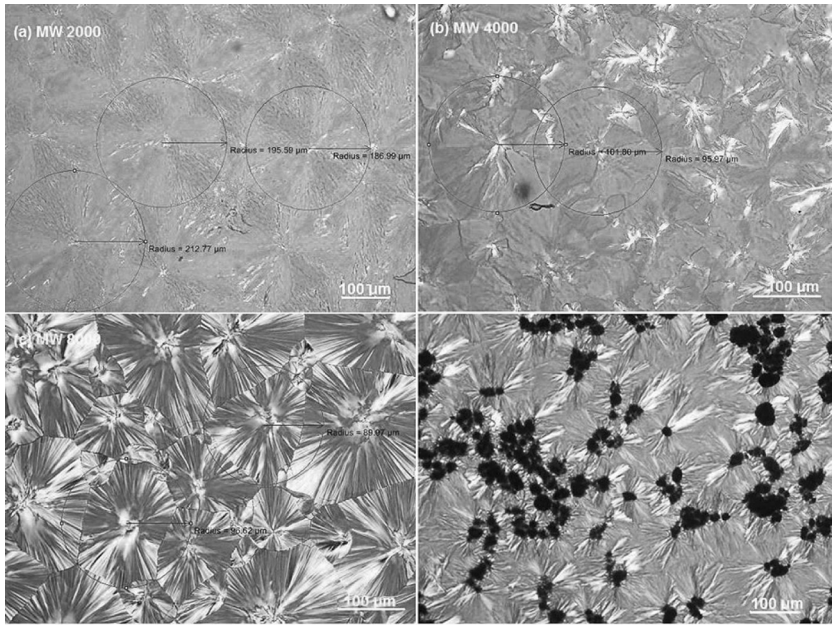

Figure 10. POM of PCL with different MW: (a) 2000, (b) 4000, (c) 8000, and (d) PCL (MW 4000)/f-MWNT composite after crystallization at 35°C for 30 min from their melts.

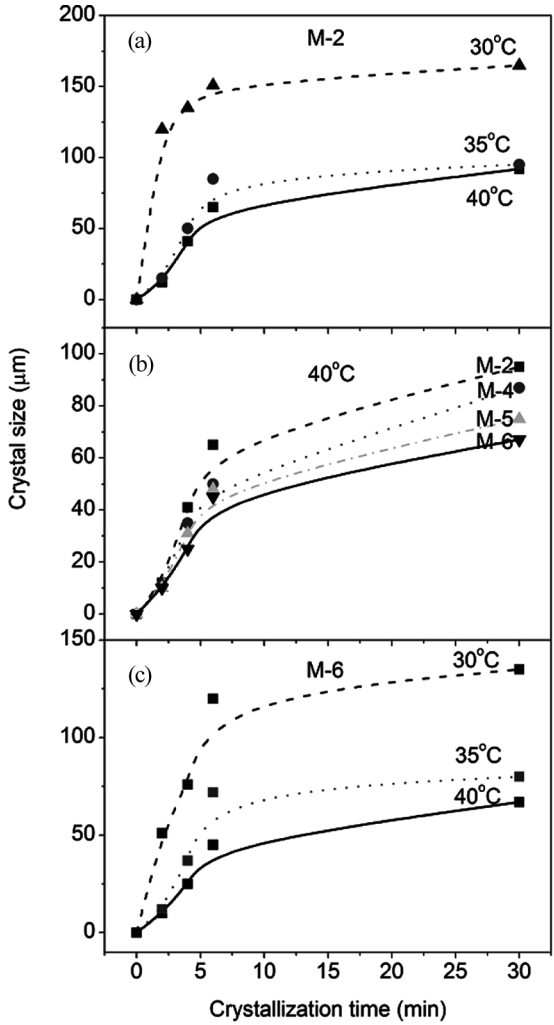

Figure 11. Variation of crystal size with (a) temperature for M-2 sample, (b) wt.% of f-MWNTs at 40°C, and (c) temperature for M-6 composite.

82.15 μm. Thus, with the addition of f-MWNTs to PCL, much smaller spherulites are observed because of the increasing nucleation density in the PCL matrix in the presence of f-MWNTs. Here the spherulite structure contains f-MWNTs at its center, indicating the nucleating action of f-MWNTs in the crystallization process. It is also found that as the weight proportion of f-MWNTs increases in the composites, the crystal size decreases (figure not shown).

Effect of Temperature

With an increase of crystallization temperature both for the neat PCL (Figure 11(a)) and the composites (Figure 11(b), (c)), there is a decreasing trend of the crystal size. At higher temperatures, the polymeric chains have higher kinetic energy so they are reluctant to be crystallized.

CONCLUSIONS

PCL reacted successfully with acylchloride functionalized MWNTs (f-MWNTs) via melt mixing at 65°C for 12 h, and the reaction was confirmed by FT-IR and SEM studies. Isothermal crystallization behavior of neat PCL and PCL/f-MWNTs composites, studied at three different temperatures (30°, 35°, and 40°C) by DSC, showed that the crystallization process proceeded in more than three modes for the neat PCL, whereas crystal growth resulted in mixed two-dimensional and three-dimensional growth for the composites. The DSC isotherm showed that the introduction of f-MWNTs into PCL induced a heterogeneous nucleation in the crystallization growth process, thereby lowering its activation energy. POM showed spherulite structure of neat PCL, whereas the composites showed spherulitic structure with f-MWNTs at its center, indicating clearly the nucleating action of f-MWNTs in the crystallization process. The spherulite size decreased but its number increased with increasing weight proportion of f-MWNTs and MW of PCL.

REFERENCES

[1] Iijima, S. (1991). Helical microtubules of graphitic carbon. *Nature* **354**, 56–58.
[2] Hu, Y., J. Shen, C. Qin, L. Wu, B. Zhang, and M. Ye. (2009). Synthesis and properties of the amino-functionalized multiple-walled carbon nanotubes/polyimide nanocomposites. *Polym. Compos.* **30**, 374–380.
[3] Choi, W. J., R. L. Powell, and D. S. Kim. (2009). Curing behavior and properties of epoxy nanocomposites with amine functionalized multiwall carbon nanotubes. *Polym. Compos.* **30**, 415–421.
[4] Lu, J., J. B. Zang, S. X. Shan, H. Huang, and Y. H. Wang. (2008). Synthesis and characterization of core-shell structural MWNT-zirconia nanocomposites. *Nano Lett.* **8**, 4070–4074.
[5] Li, M. K., M. Lu, L. B. Kong, X. Y. Guo, and H. L. Li. (2003). The synthesis of MWNTs/SWNTs multiple phase nanowire arrays in porous anodic aluminum oxide templates. *Mater. Sci. Eng. A.* **354**, 92–96.
[6] Yun, S., and J. Kim. (2007). A bending electro-active paper actuator made by mixing multi-walled carbon nanotubes and cellulose. *Smart Mater. Struc.* **16**, 1471–1476.

[7] Hughes, M., and G. M. Spinks. (2005). Multiwalled carbon nanotube actuators. *Adv. Mater.* **17**, 443–446.
[8] Rakhi, R. B., K. Sethupathi, and S. Ramaprabhu. (2009). Electron field emitters based on multi-walled carbon nanotubes coated with conducting polymer/metal/metal-oxide composites. *J. Exp. Nanosci.* **4**, 67–76.
[9] Lee, S. B., A. S. Teh, K. B. K. Teo, M. Chhowalla, D. G. Hasko, W. I. Milne, G. A. J. Amaratunga, and H. Ahmed. (2003). Fabrication of carbon nanotube lateral field emitters. *Nanotechnology* **14**, 192–195.
[10] Hu, C., H. Liao, F. Li, J. Xiang, W. Li, S. Duo, and M. Li. (2008). Noncovalent functionalization of multi-walled carbon nanotubes with siloxane polyether copolymer. *Mater. Lett.* **62**, 2585–2588.
[11] Jeong, J. S., J. S. Moon, S. Y. Jeon, J. H. Park, P. S. Alegaonkar, and J. B. Yoo. (2007). Mechanical properties of electrospun PVA/MWNTs composite nanofibers. *Thin Solid Films* **515**, 5136–5141.
[12] Seo, M. K., and S. J. Park. (2009). Influence of functionalization on physicochemical properties of multi-walled carbon nanotubes/epoxy matrix nanocomposites. *Bull. Korean Chem. Soc.* **30**, 124–128.
[13] Zhang, W. D., L. Shen, I. Y. Phang, and T. Liu. (2004). Carbon nanotubes reinforced nylon-6 composite prepared by simple melt-compounding. *Macromolecules* **37**, 256–259.
[14] Vaaben, S. R., A. Aguilar, F. Avalos, and L. F. Ramos-de Valle. (2008). Carbon nanoparticles as effective nucleating agents for polypropylene. *J. Therm. Anal. Calorim.* **93**, 947–952.
[15] Jana, R. N., and J. W. Cho. (2008). Thermal stability and molecular interaction of polyurethane nanocomposites prepared by *in situ* polymerization with functionalized multi walled carbon nanotubes. *J. Appl. Polym. Sci.* **108**, 2857–2864.
[16] He, Y., T. Masuda, A. Cao, N. Yoshie, Y. Doi, and Y. Inoue. (1999). Thermal, crystallization, and biodegradation behavior of poly(3-hydroxybutyrate) blends with poly(butylene succinate-*co*-butylene adipate) and poly (butylene succinate-*co*-ε-caprolactone). *Polym. J.* **31**, 184–192.
[17] Wei, M., X. Shuai, and A. E. Tonelli. (2003). Melting and crystallization behaviors of biodegradable polymers enzymatically coalesced from their cyclodextrin inclusion complexes. *Biomacromolecules* **4**, 783–792.
[18] Jabarin, S. A. (1987). Crystallization kinetics of polyethylene terephthalate. I. Isothermal crystallization from the melt. *J. Appl. Polym. Sci.* **34**, 85–96.
[19] Vilanova, P. C., S. M. Robas, and G. M. Guzman. (1985). Isothermal crystallization of poly(ethylene-terephthalate) of low molecular weight by differential scanning calorimetry: 1. Crystallization kinetics. *Polymer* **26**, 423–428.
[20] Bicerano, J. (1998). Crystallization of polypropylene and poly(ethylene terephthalate). *J. Macromol. Sci. Part C Rev. Macromol. Chem. Phys.* **C38**, 391–479.
[21] Lambert, W. S., and P. J. Phillips. (1996). Isothermal crystallization of poly(ethylene-terephthalate) of low molecular weight by differential scanning calorimetry: 1. Crystallization kinetics. *Polymer* **37**, 3585–3591.
[22] Chaudhari, A., J. D. Ekhe, and S. Deo. (2006). Non-isothermal crystallization behavior of lignin-filled polyethylene terepthalate (PET). *Int. J. Polym. Anal. Charact.* **11**, 197–207.

[23] Maxfield, J., and L. Mandelkern. (1972). Molecular weight dependence of the crystallization kinetics of linear polyethylene. I. Experimental results. *Macromolecules* **5**, 147–157.
[24] Shan, H., and G. C. Lickfield. (2007). Crystallization kinetics study of polyethylene. *Int. J. Polym. Anal. Charact.* **12**, 327–338.
[25] Shan, H., J. L. White, and A. W. deGroot. (2007). Comparison of crystallization and melting characteristics of quiescent and melt-spun poly(ethylene-co-octene) copolymers. *Int. J. Polym. Anal. Charact.* **12**, 231–249.
[26] Shan, H., J. L. White, and A. W. deGroot. (2006). Simple ways to characterize non-isothermal crystallization of homogeneous poly(ethylene-1-co-octene) copolymer. *Int. J. Polym. Anal. Charact.* **11**, 323–336.
[27] Risch, B. G., S. Srintvas, G. Wikes, J. F. Geilel, C. Ash, S. White, and M. Hicks. (1996). Crystallization behaviour of poly(*p*-phenylene sulfide): Effects of molecular weight fractionation and endgroup counter-ion. *Polymer* **37**, 3623–3636.
[28] De Carvalho, B., and R. E. S. Bretas. (1999). Quiescent crystallization kinetics and morphology of i-PP resins for injection molding. II. Nonisothermal crystallization as a function of molecular weight. *J. Appl. Polym. Sci.* **72** (13), 1733–1740.
[29] Alamo, R., J. G. Fatou, and J. Guzman. (1982). Crystallization of polyformals: 1. Crystallization kinetics of poly(1,3-dioxolane). *Polymer* **23**, 374–378.
[30] Wu, T. M., and E. C. Chen. (2006). Crystallization behavior of poly (ε-caprolactone)/multiwalled carbon nanotube composites. *J. Polym. Sci. Part B Polym. Phys.* **44**, 598–606.
[31] Ming, W. T., and C. E. Chiang. (2006). Isothermal and nonisothermal crystallization kinetics of poly (ε-caprolactone)/multi-walled carbon nanotube composites. *Polym. Eng. Sci.* **46**, 1309–1317.
[32] Chiang, C. E., and W. T. Ming. (2007). Isothermal crystallization kinetics and thermal behavior of poly (ε-caprolactone)/multi-walled carbon nanotube composites. *Polym. Degradation Stab.* **92**, 1009–1015.
[33] Jana, R. N., and J. W. Cho. (2008). Thermal stability, crystallization behavior, and phase morphology of poly (ε-caprolactone) diol-grafted-multiwalled carbon nanotubes. *J. Appl. Polym. Sci.* **110**, 1550–1558.
[34] Jana, R. N., H. J. Yoo, and J. W. Cho. (2008). Synthesis and properties of shape memory polyurethane nanocomposites reinforced with poly (ε-caprolactone)-grafted carbon nanotubes. *Fibers Polym.* **9**, 247–254.
[35] Kumar, N. A., S. H. Kim, B. G. Cho, K. T. Lim, and Y. T. Jeong. (2009). Surface functionalization of multi walled carbon nanotubes with poly (3,4-propylene dioxythiophene) and preparation of its random copolymers: New hybrid materials. *Colloid Polym. Sci.* **287**, 97–102.
[36] Wu, H. L., C. M. Ma, Y. T. Yang, H. C. Kuan, C. C. Yang, and C. L. Chiang. (2006). Morphology, electrical resistance, electromagnetic interference shielding and mechanical properties of functionalized MWNT and poly(urea urethane) nanocomposites. *J. Polym. Sci. Part B Polym. Phys.* **44**, 1096–1105.
[37] Lee, C. H., J. Y. Liu, S. L. Chen, and Y. Z. Wang. (2007). Miscibility and properties of acid-treated multi-walled carbon nanotubes/polyurethane nanocomposites. *Polym. J.* **39**, 138–146.

[38] Lorenzo, A. T., M. L. Arnal, J. Albuerne, and A. J. Muller. (2007). DSC isothermal polymer crystallization kinetics measurements and the use of the Avrami equation to fit the data: Guidelines to avoid common problems. *Polym. Test.* **26**, 222–231.
[39] Chen, J. H., B. X. Yao, W. B. Su, and Y. B. Yang. (2007). Isothermal crystallization behavior of isotactic polypropylene blended with small loading of polyhedral oligomeric silsesquioxane. *Polymer* **48** (6), 1756–1769.